

Néel to dimer transition in spin- S antiferromagnets: Comparing bond operator theory with quantum Monte Carlo simulations for bilayer Heisenberg models

R. Ganesh,¹ Sergei V. Isakov,² and Arun Paramekanti^{1,3}¹*Department of Physics, University of Toronto, Toronto, Ontario, Canada M5S 1A7*²*Theoretische Physik, ETH Zurich, CH-8093 Zurich, Switzerland*³*Canadian Institute for Advanced Research, Toronto, Ontario, Canada M5G 1Z8*

(Received 20 September 2011; revised manuscript received 1 November 2011; published 7 December 2011)

We study the Néel to dimer transition driven by interlayer exchange coupling in spin- S Heisenberg antiferromagnets on bilayer square and honeycomb lattices for $S = 1/2, 1$, and $3/2$. Using exact stochastic series expansion quantum Monte Carlo (QMC) calculations, we find that the critical value of the interlayer coupling, $J_{\perp c}[S]$, increases with increasing S , with clear evidence that the transition is in the $O(3)$ universality class for all S . Using bond operator mean-field theory restricted to singlet and triplet states, we find $J_{\perp c}[S] \propto S(S+1)$, in qualitative accord with QMC, but the resulting $J_{\perp c}[S]$ is significantly smaller than the QMC value. For $S = 1/2$, incorporating triplet-triplet interactions within a variational approach yields a critical interlayer coupling, which agrees well with QMC. For higher spin, we argue that it is crucial to account for the high-energy quintet modes, and we show that including these within a perturbative scheme leads to reasonable agreement with QMC results for $S = 1$ and $3/2$. We discuss the broad implications of our results for systems such as the triangular lattice $S = 1$ dimer compound $\text{Ba}_3\text{Mn}_2\text{O}_8$ and the $S = 3/2$ bilayer honeycomb material $\text{Bi}_3\text{Mn}_4\text{O}_{12}(\text{NO}_3)$.

DOI: 10.1103/PhysRevB.84.214412

PACS number(s): 75.10.Jm, 75.30.Kz, 75.50.Ee, 73.21.Ac

I. INTRODUCTION

Spin dimer compounds provide the simplest realization of a magnetically disordered ground state—one in which strongly coupled pairs of spins entangle to form singlets. Such systems are also of great interest since they undergo magnetic-field-induced spin ordering via a quantum phase transition, which is analogous to Bose-Einstein condensation.^{1–4} There are many well-known spin dimer compounds^{5–8} and well studied model Hamiltonians^{9–12} exhibiting such physics for $S = 1/2$ spins. However, ongoing experiments on higher spin systems, such as the $S = 1$ triangular lattice dimer compound¹³ $\text{Ba}_3\text{Mn}_2\text{O}_8$, point to a need to better understand higher spin generalizations and instabilities of such dimer states driven by interdimer interactions.

Here, we explore this issue using a simple model that exhibits such a dimerized ground state, namely the bilayer Heisenberg antiferromagnet, with a Hamiltonian given by

$$H = J_{\perp} \sum_i \mathbf{S}_{i,1} \cdot \mathbf{S}_{i,2} + J_1 \sum_{\langle ij \rangle} \sum_{\ell=1,2} \mathbf{S}_{i,\ell} \cdot \mathbf{S}_{j,\ell}. \quad (1)$$

Here, i labels sites in one layer, $\ell = 1, 2$ is the layer index, and $\langle ij \rangle$ represents nearest-neighbor pairs of spins within each layer. For $J_{\perp} \gg J_1$, the first term in H dominates and the ground state is composed of isolated interlayer singlets with $\mathbf{S}_{i,1} + \mathbf{S}_{i,2} = 0$ for every i . If $J_{\perp} \ll J_1$, the system will order magnetically provided the second (intralayer) term in the Hamiltonian is not too frustrated by the lattice geometry. Here, we restrict our attention to cases in which each layer is itself a bipartite lattice so that the ground state for $J_{\perp} \ll J_1$ has long-range Néel order [see Fig. 1(a)]. This model Hamiltonian has been studied extensively for the $S = 1/2$ square lattice bilayer.^{11,14–18} The effects of disorder, induced by site dilution, have also been explored.¹⁹ However, there has been relatively little work on understanding the higher spin generalizations of the Hamiltonian in Eq. (1). The spin- S square lattice

bilayer has been studied using Schwinger boson mean-field theory²⁰ and series expansions.²¹ Variants of this spin- S model have been argued to support novel spin solid phases in three dimensions.²² In this paper, we study this Hamiltonian for $S = 1/2, 1$, and $3/2$ spins on square and honeycomb bilayers using exact quantum Monte Carlo simulation algorithms²³ and approximate analyses based on a bond operator method generalized to arbitrary spin.²⁴

Our main results are as follows. (i) Using exact stochastic series expansion quantum Monte Carlo (QMC) calculations, we find a Néel to dimer transition with increasing J_{\perp} that is in the $O(3)$ universality class for all the models we have studied. (ii) The critical value of the interlayer coupling, $J_{\perp c}[S]$, for the Néel to dimer transition is found to increase for higher spin. Using a bond operator mean-field theory restricted to singlet and triplet states, we find $J_{\perp c}[S] \propto S(S+1)$, in qualitative accord with QMC results. However, there is a quantitative discrepancy between the mean field $J_{\perp c}[S]$ and its QMC value, which becomes more significant for higher spin. (iii) For $S = 1/2$, we show that taking into account triplet-triplet interactions within a variational approach brings the $J_{\perp c}[S]$ value close to the QMC result. For higher spin, we show that the dominant corrections to the critical point arise from the high-energy quintet modes, and direct triplet-triplet interactions are less important. Incorporating the quintet excitations within a perturbative treatment is shown to yield a critical interlayer coupling that is in good agreement with QMC results for $S = 1$ and $3/2$. We discuss the broad implications of our results for high-spin antiferromagnets such as the triangular lattice $S = 1$ dimer compound¹³ $\text{Ba}_3\text{Mn}_2\text{O}_8$ and the $S = 3/2$ bilayer honeycomb material²⁵ $\text{Bi}_3\text{Mn}_4\text{O}_{12}(\text{NO}_3)$.

This paper is organized as follows. Section II contains results from the QMC simulations on the phase diagram of the honeycomb and square lattice bilayer models for $S = 1/2, 1$, and $3/2$. In Sec. III, we outline the bond operator formalism generalized to the case of spin S . Section IV gives bond operator mean-field theory results for the square and honeycomb

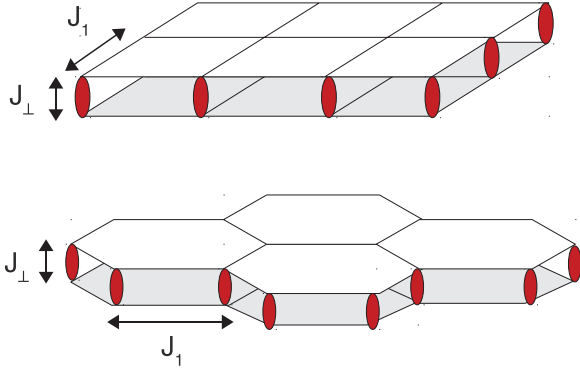


FIG. 1. (Color online) The interlayer dimer state on square and honeycomb bilayers with singlet correlations between layers. The in-plane exchange J_1 and the interplane exchange J_\perp act as shown.

lattice models. Section V discusses the variational approach that we use to take into account corrections beyond mean-field theory. Section VI analyzes the $S = 1/2$ model including the effect of triplet-triplet interactions, while Sec. VII contains a treatment of the dominant quintet corrections for $S > 1/2$. We end with a discussion in Sec. VIII. Details are contained in the Appendixes.

II. QUANTUM MONTE CARLO SIMULATIONS

The bilayer honeycomb and square lattices are bipartite lattices which can be split into two sublattices A and B, with every lattice bond being a link between sites belonging to different sublattices. This ensures that there is no sign problem, so that the model in Eq. (1) is amenable to quantum Monte Carlo simulations. We perform quantum Monte Carlo simulations for $S = 1/2, 1$, and $3/2$ on the bilayer square (of linear system size $L = 12, 16, 24, 32$, and 40) and bilayer honeycomb ($L = 12, 18, 24, 30$, and 36) lattices using the stochastic series expansion algorithm.²³ For $S = 1$ and $3/2$, simulations are performed with modified worm weights, which lead to a slightly more efficient algorithm, as in Ref. 26. At large enough ratio J_\perp/J_1 , the system undergoes a quantum phase transition from a Néel state to a dimerized paramagnetic state. To locate the quantum critical points, we perform finite-size scaling analysis of the superfluid density and the staggered magnetization density squared. We measure the superfluid density ρ_s by measuring winding number fluctuations,²⁷

$$\rho_s = T \frac{\langle W_1^2 + W_2^2 \rangle}{2J_1},$$

where $W_{1,2}$ are the winding numbers in two spatial directions and T is the temperature. The staggered magnetization density squared is given by

$$|m_s|^2 = 3 \left[\frac{1}{N} \sum_i^N (-1)^p S_i^z \right]^2,$$

where $(-1)^p = 1$ for lattice sites from sublattice A, $(-1)^p = -1$ for sites from sublattice B, and N is the number of lattice sites. In the vicinity of a continuous phase transition, the

superfluid density scales as

$$\rho_s = L^{2-d-z} F \left([K - K_c] L^{1/\nu}, \frac{1}{TL^z} \right),$$

where L is the linear system size, $d = 2$ is the dimensionality of the system, T is the temperature, $[K - K_c] \equiv [(J_\perp - J_{\perp c})/J_1]$ is the distance from the critical point $J_{\perp c}/J_1$, and ν is the correlation length critical exponent. The staggered magnetization density squared scales as

$$|m_s|^2 = L^{-2\beta/\nu} M \left([K - K_c] L^{1/\nu}, \frac{1}{TL^z} \right),$$

where β is the critical exponent. If one plots $\rho_s L^z$ as a function of J_\perp/J_1 at a large enough and fixed value of $1/(TL^z)$, then the curves for different system sizes should cross at the critical point $J_{\perp c}/J_1$. If one plots $\rho_s L^z$ as a function of $[K - K_c] L^{1/\nu}$, with appropriately chosen values of the critical exponents and K_c , the curves for different system sizes should collapse onto the universal curve given by the function F .

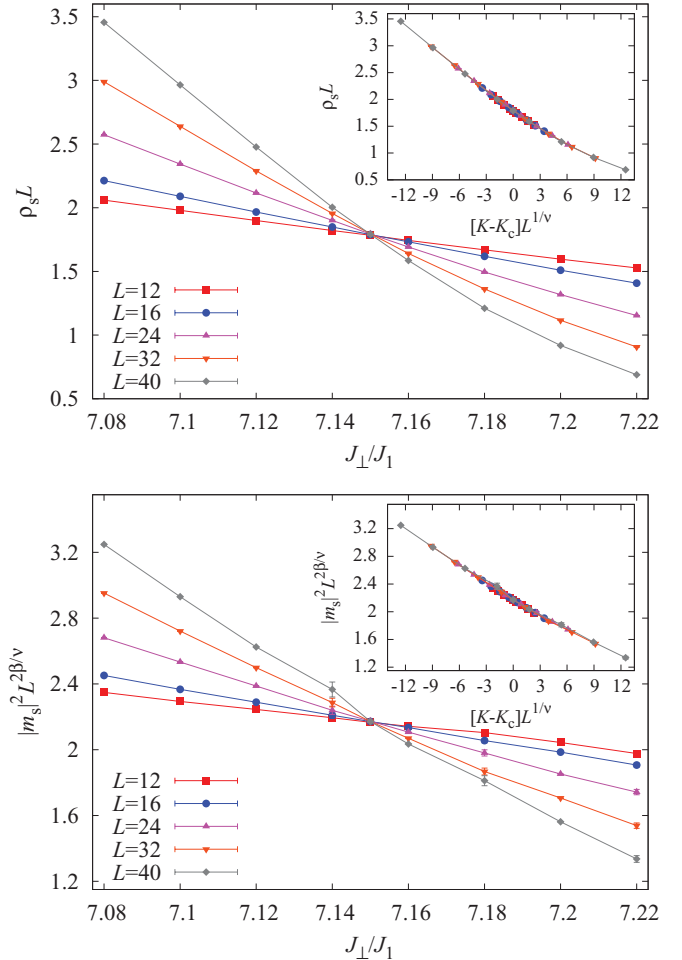


FIG. 2. (Color online) Scaling of the superfluid density (upper panel) and of the staggered magnetization density squared (lower panel) for the $S = 1$ antiferromagnet on the bilayer square lattice. The curves cross at a distinct point around $J_\perp/J_1 = 7.15$. The insets show the corresponding data collapse for $z = 1$, $\nu = 0.7112$, $\beta = 0.3689$, and $J_{\perp c}/J_1 = 7.15$. Lines guide the eye. The error bars are smaller than the symbol size if not visible.

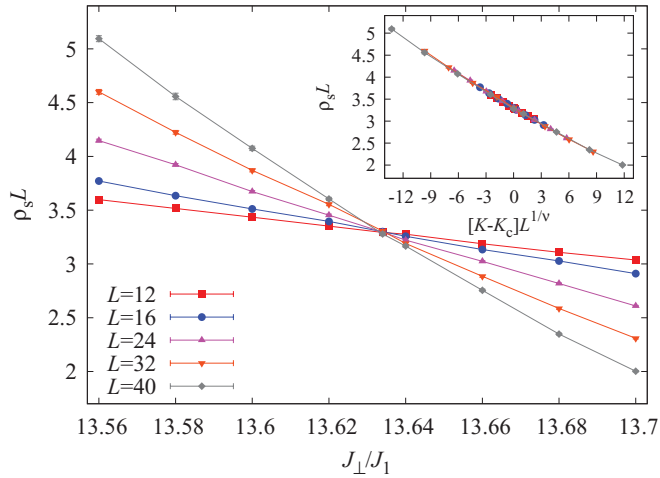


FIG. 3. (Color online) Scaling of the superfluid density for the $S = 3/2$ antiferromagnet on the bilayer square lattice. The curves cross at a distinct point around $J_{\perp}/J_1 = 13.634$. The inset shows the corresponding data collapse for $z = 1$, $\nu = 0.7112$, and $J_{\perp c}/J_1 = 13.634$. Lines guide the eye. The error bars are smaller than the symbol size if not visible.

Similarly, $|m_s|^2 L^{2\beta/\nu}$ as a function of J_{\perp}/J_1 should have a distinct crossing point at the critical point, and $|m_s|^2 L^{2\beta/\nu}$ as a function of $[K - K_c] L^{1/\nu}$ should collapse onto the universal curve given by the function M . We perform simulations at a fixed aspect ratio $T = J_1/2L$.

A. Square lattice

The quantum critical point for the $S = 1/2$ bilayer quantum antiferromagnet on the square lattice was found in Refs. 11 and 28, $J_{\perp c}/J_1 = 2.5220(1)$. In the present work, we find that the quantum critical points are located at $J_{\perp c}/J_1 = 7.150(2)$ for $S = 1$ and at $J_{\perp c}/J_1 = 13.634(3)$ for $S = 3/2$. The data scale very well with the critical exponents $\nu = 0.7112$ and $\beta = 0.3689$ of the $O(3)$ universality class²⁹ for any value of spin. The crossing points and data collapse for $S = 1$ and $3/2$ are shown in Figs. 2 and 3. Note that we do not show the scaling of the magnetization density squared for $S = 3/2$ because the data points are too noisy.

B. Honeycomb lattice

We find that for the honeycomb lattice, the quantum critical points are located at $J_{\perp c}/J_1 = 1.645(1)$ for $S = 1/2$, $J_{\perp c}/J_1 = 4.785(1)$ for $S = 1$, and $J_{\perp c}/J_1 = 9.194(3)$ for $S = 3/2$. The data scale very well with the critical exponents $\nu = 0.7112$ and $\beta = 0.3689$ of the $O(3)$ universality class²⁹ for any value of spin. The crossing points and data collapse for $S = 1$ and $3/2$ are shown in Figs. 4 and 5. We do not show the scaling of the magnetization density squared for $S = 3/2$ because the data points are too noisy.

C. Critical point as a function of spin

In Fig. 6, we show the quantum critical points $J_{\perp c}/J_1$ as functions of $S(S + 1)$ for the bilayer square and honeycomb lattices. We find that $J_{\perp c}/J_1[S]$ is a linear function of $S(S + 1)$. In the following sections, we will attempt to make sense of

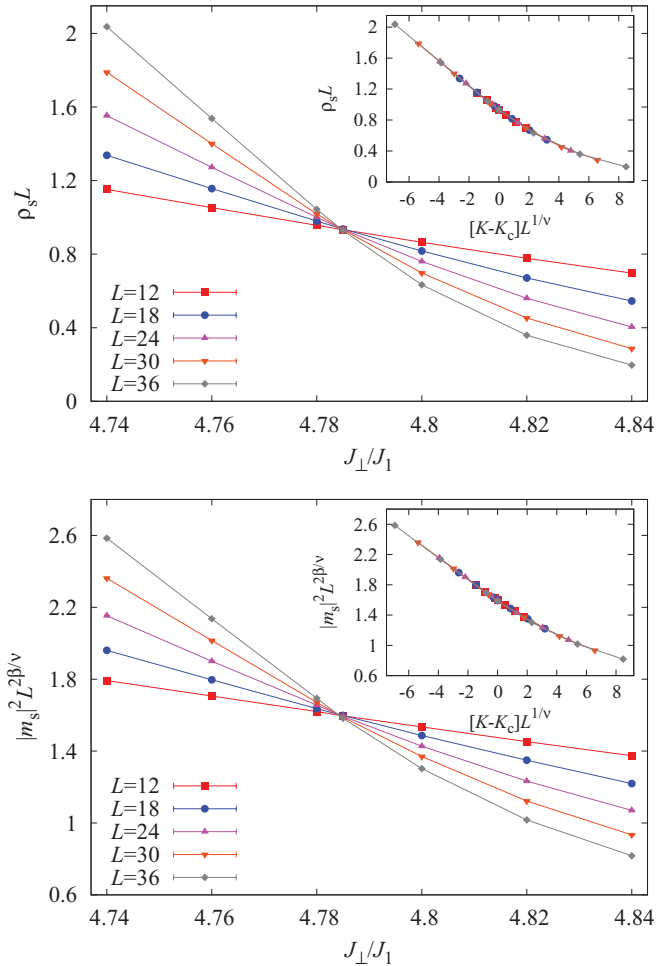


FIG. 4. (Color online) Scaling of the superfluid density (upper panel) and of the staggered magnetization density squared (lower panel) for the $S = 1$ antiferromagnet on the bilayer honeycomb lattice. The curves cross at a distinct point around $J_{\perp}/J_1 = 4.785$. The insets show the corresponding data collapse for $z = 1$, $\nu = 0.7112$, $\beta = 0.3689$, and $J_{\perp c}/J_1 = 4.785$. Lines guide the eye. The error bars are smaller than the symbol size if not visible.

these QMC results using an extension of the bond operator theory of the dimerized state and its instability to Néel order.

III. BOND OPERATOR REPRESENTATION

An elegant approach that allows us to understand the physics of the dimer ground state and its magnetic ordering instabilities is the bond operator formalism, which was first proposed for $S = 1/2$ antiferromagnets.³⁰ In this scheme, the spin operators are represented in a new basis consisting of singlet and triplet states on the interlayer bonds $(i, 1)-(i, 2)$. In the limit where the intralayer coupling $J_1 = 0$, the ground state consists of localized singlets on these bonds, with a gap J_{\perp} to the triplet excitations. A nonzero J_1 allows a pair of neighboring bonds $(i, 1)-(i, 2)$ and $(j, 1)-(j, 2)$ to exchange their singlet/triplet character. Such a “triplet hopping” process converts the localized triplet modes into dispersing “triplons,” with threefold-degenerate bands due to the underlying $SU(2)$ symmetry of the Hamiltonian. In this picture, the dimer to Néel transition is an $O(3)$ transition driven by the condensation of

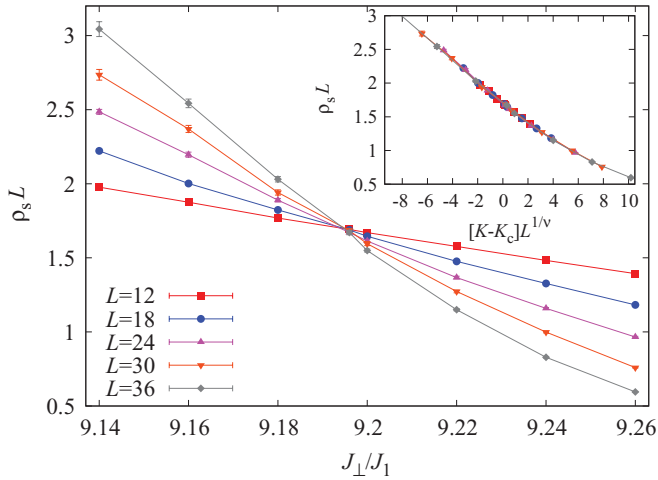


FIG. 5. (Color online) Scaling of the superfluid density for the $S = 3/2$ antiferromagnet on the bilayer honeycomb lattice. The curves cross at a distinct point around $J_{\perp}/J_1 = 9.194$. The inset shows the corresponding data collapse for $z = 1$, $\nu = 0.7112$, and $J_{\perp c}/J_1 = 9.194$. Lines guide the eye. The error bars are smaller than the symbol size if not visible.

triplon modes at a certain wave vector where the dispersion minimum hits zero. Generalizations of this approach to spin-1 magnets have been proposed earlier.^{31,32} Here, we adopt a recent generalization of the bond operator method to arbitrary spin²⁴ to study bilayer Heisenberg antiferromagnets.

In a spin- S bilayer system, in the limit $J_{\perp} \gg J_1$, we have isolated interlayer bonds. The bond can be in one of the following states: a singlet, a threefold-degenerate triplet, a fivefold-degenerate quintet, etc. We introduce one boson for each of these states:

$$\begin{aligned} |s_i\rangle &\equiv s_i^{\dagger}|0\rangle, \\ |t_{i,m \in \{-1,0,1\}}\rangle &\equiv t_{i,m}^{\dagger}|0\rangle, \\ |q_{i,m \in \{-2,\dots,2\}}\rangle &\equiv q_{i,m}^{\dagger}|0\rangle, \\ &\vdots \end{aligned}$$

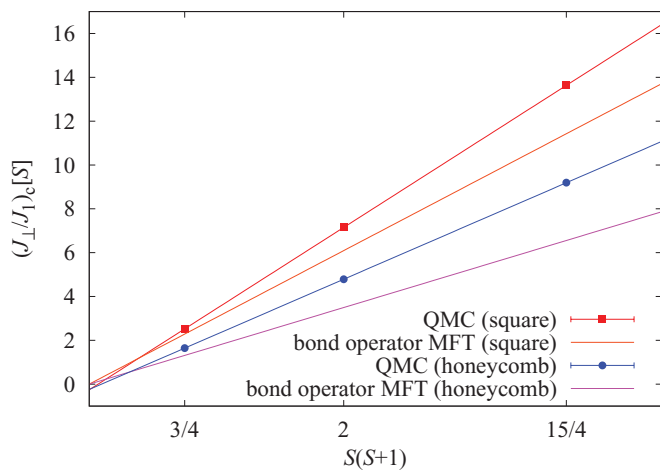


FIG. 6. (Color online) $J_{\perp c}/J_1[S]$ as a function of $S(S+1)$ for the bilayer square and honeycomb lattices. Lines are linear fits. Note that the curves cross approximately at $S(S+1) = 0$.

The index i here runs over all interlayer bonds, and m labels the S_z component of the total spin on the interlayer bond. These boson operators form the basis for a bond operator representation. To restrict to the physical Hilbert space of spins, every interlayer bond should have exactly one boson,

$$s_i^{\dagger}s_i + \sum_{m=-1,0,1} t_{i,m}^{\dagger}t_{i,m} + \sum_{n=-2,\dots,2} q_{i,n}^{\dagger}q_{i,n} + \dots = 1. \quad (2)$$

In terms of bond operators, the exchange interaction on an interlayer bond is given by

$$\begin{aligned} J_{\perp} \mathbf{S}_{i,1} \cdot \mathbf{S}_{i,2} &= \varepsilon_s s_i^{\dagger}s_i + \varepsilon_t \sum_{m=-1,0,1} t_{i,m}^{\dagger}t_{i,m} \\ &+ \varepsilon_q \sum_{m=-2,\dots,2} q_{i,m}^{\dagger}q_{i,m} + \dots, \quad (3) \end{aligned}$$

where $\varepsilon_s = -J_{\perp}S(S+1)$, $\varepsilon_t = J_{\perp}\{1 - S(S+1)\}$, and $\varepsilon_q = J_{\perp}\{3 - S(S+1)\}$.

Bond operator theory reexpresses the spin operators and their interactions in terms of these bond bosons. In the limit $J_{\perp} \gg J_1$, the singlets, triplets, quintets, etc. form a hierarchy with the energy spacing between each tier of order J_{\perp} . In this paper, we restrict our analysis to the low-energy subspace of singlets, triplets, and quintets on a bond, and we neglect higher spin states as they are much higher in energy.

We first turn to the usual bond operator mean-field theory retaining only singlet and triplet modes, ignoring triplet interactions and higher excited states and imposing the constraint in Eq. (2) on average. We then consider, in turn, the effect of triplet-triplet interactions for $S = 1/2$ and the effect of quintet states for $S > 1/2$. For convenience of notation, we henceforth set $J_1 = 1$, thus measuring J_{\perp} in units of J_1 .

IV. SINGLET-TRIPLET MEAN-FIELD THEORY

At mean-field level, the interlayer dimer state is described by a uniform condensate of the singlet bosons, with $\langle s_i \rangle = \langle s_i^{\dagger} \rangle = \bar{s}$. Retaining only triplet excitations, the spin operators at each site are given by²⁴

$$\begin{aligned} S_{i,\ell}^+ &= (-1)^{\ell} \sqrt{\frac{2S(S+1)}{3}} \bar{s} \{t_{i,-1} - t_{i,1}^{\dagger}\} \\ &+ \frac{1}{\sqrt{2}} \{t_{i,1}^{\dagger}t_{i,0} + t_{i,0}^{\dagger}t_{i,-1}\}, \quad (4) \\ S_{i,\ell}^z &= (-1)^{\ell} \sqrt{\frac{S(S+1)}{3}} \bar{s} \{t_{i,0} + t_{i,0}^{\dagger}\} \\ &+ \frac{1}{2} \{t_{i,1}^{\dagger}t_{i,1} - t_{i,-1}^{\dagger}t_{i,-1}\}. \quad (5) \end{aligned}$$

Using these expressions, the Hamiltonian takes the form

$$\begin{aligned} H_{\text{mf}} &= \varepsilon_s N_{\perp} \bar{s}^2 + \varepsilon_t \sum_{i,m} t_{i,m}^{\dagger}t_{i,m} - \mu \sum_i \left(\sum_m t_{i,m}^{\dagger}t_{i,m} + \bar{s}^2 - 1 \right) \\ &+ \frac{2S(S+1)}{3} \bar{s}^2 \sum_{\langle i,j \rangle} \{t_{i,0} + t_{i,0}^{\dagger}\} \{t_{j,0} + t_{j,0}^{\dagger}\} \\ &+ (\{t_{i,-1} - t_{i,1}^{\dagger}\} \{t_{j,-1}^{\dagger} - t_{j,1}\} + \text{H.c.}), \quad (6) \end{aligned}$$

where μ is a Lagrange multiplier that enforces the constraint in Eq. (2) on average. N_{\perp} is the number of interlayer bonds.

We have dropped quartic terms in the triplet operators (which corresponds to ignoring triplet-triplet interactions).

In the rest of this paper, we use the following two basis sets to represent triplet states: $\{|t_{-1}\rangle_i, |t_0\rangle_i, |t_1\rangle_i\}$ or $\{|t_x\rangle_i, |t_y\rangle_i, |t_z\rangle_i\}$. The former basis labels states by the z projection of spin. The latter labels each state by the direction in which its spin projection is zero. We can go from one basis to another using $|t_0\rangle_i = |t_z\rangle_i$ and $|t_{\pm 1}\rangle_i = (\mp|t_x\rangle_i - i|t_y\rangle_i)/\sqrt{2}$. Below, we will use the index m to represent an element of the first basis and u to represent an element of the second.

A. Square lattice bilayer

A top view of the square lattice bilayer with the relevant primitive lattice vectors is shown in Fig. 7. At mean-field level, the Hamiltonian of Eq. (1) may be written as

$$H_{\square}^{(0)} = -J_{\perp} N_{\perp} S(S+1) \bar{s}^2 - \mu \bar{s}^2 N_{\perp} + \mu N_{\perp} - \frac{3N_{\perp} A}{2} + \sum_{\mathbf{k}, u \in \{x, y, z\}}' \psi_{\mathbf{k}, u}^{\dagger} \begin{pmatrix} A + 2\epsilon_{\mathbf{k}} & 2\epsilon_{\mathbf{k}} \\ 2\epsilon_{\mathbf{k}} & A + 2\epsilon_{\mathbf{k}} \end{pmatrix} \psi_{\mathbf{k}, u}, \quad (7)$$

where $\psi_{\mathbf{k}, u} = [t_{\mathbf{k}, u} \quad t_{-\mathbf{k}, u}^{\dagger}]^T$. The primed summation indicates that if \mathbf{k} is included in the sum, then $-\mathbf{k}$ is excluded. The coefficients in the Hamiltonian matrix are

$$A = J_{\perp} \{1 - S(S+1)\} - \mu, \quad (8)$$

$$\epsilon_{\mathbf{k}} = \frac{2S(S+1)}{3} \bar{s}^2 [\cos(k_x) + \cos(k_y)]. \quad (9)$$

Diagonalizing this Hamiltonian matrix by a bosonic Bogoliubov transformation (see Appendix A), we obtain eigenvalues $\lambda_{\mathbf{k}} = \sqrt{A(A + 4\epsilon_{\mathbf{k}})}$ for the energies of the independent ‘‘triplon’’ modes. Each of these modes adds a zero-point contribution to the ground-state energy, yielding

$$E_{\square}^{(0)} = -J_{\perp} N_{\perp} S(S+1) \bar{s}^2 - \mu \bar{s}^2 N_{\perp} + \mu N_{\perp} - \frac{3N_{\perp} A}{2} + 3 \sum_{\mathbf{k}}' \lambda_{\mathbf{k}}. \quad (10)$$

We minimize this ground-state energy with respect to μ and \bar{s} , via $\partial E_{\square}^{(0)}/\partial \mu = 0$ and $\partial E_{\square}^{(0)}/\partial \bar{s}^2 = 0$. This yields the two equations

$$\bar{s}^2 = \frac{5}{2} - \frac{3}{N_{\perp}} \sum_{\mathbf{k}}' \frac{A + 2\epsilon_{\mathbf{k}}}{\lambda_{\mathbf{k}}}, \quad (11)$$

$$\mu = -J_{\perp} S(S+1) + \frac{6}{N_{\perp}} \sum_{\mathbf{k}}' \frac{A\epsilon_{\mathbf{k}}}{\bar{s}^2 \lambda_{\mathbf{k}}}. \quad (12)$$

Using the values of \bar{s} and μ thus obtained, we may calculate the gap to triplet excitations. The dimer-Néel transition occurs when the triplon gap vanishes at $J_{\perp} = J_{\perp c}$. We have explicitly checked that triplon condensation at $\mathbf{k} = (\pi, \pi)$ yields Néel order on the bilayer. Using Eqs. (11) and (12) above, we arrive at the following two results at the critical point. (i) The value \bar{s} at the dimer-Néel critical point is independent of spin and is given by

$$\bar{s}_c^2 = \frac{5}{2} - \frac{3}{2N_{\perp}} \sum_{\mathbf{k}}' \frac{4 + (\cos k_x + \cos k_y)}{\sqrt{4 + 2(\cos k_x + \cos k_y)}}. \quad (13)$$

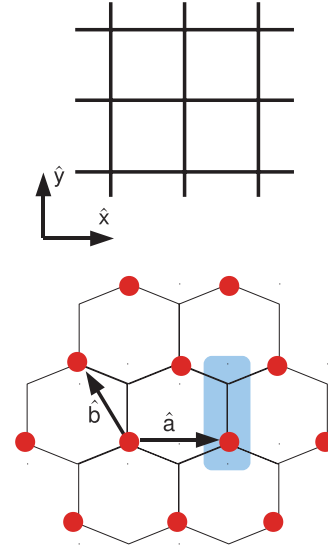


FIG. 7. (Color online) Top view of bilayers. (Top) Square lattice with primitive lattice vectors \hat{x} and \hat{y} shown. (Bottom) Honeycomb lattice. The shaded region is the unit cell composed of two sites. Sites marked with a red circle belong to the A sublattice. Unmarked sites belong to the B sublattice. The primitive lattice vectors \hat{a} and \hat{b} are shown.

A numerical evaluation shows $\bar{s}_c \approx 0.904$. (ii) We find the location of the dimer-Néel critical point,

$$J_{\perp c} = S(S+1) \left[\frac{40}{3} - \frac{32}{N_{\perp}} \sum_{\mathbf{k}}' \frac{1}{\sqrt{4 + 2(\cos k_x + \cos k_y)}} \right]. \quad (14)$$

A numerical evaluation yields $J_{\perp c} \approx 3.047S(S+1)$. For $S = 1/2$, this mean-field result, $J_{\perp c}[S = 1/2] \approx 2.286$, agrees with previous work¹⁷ and is slightly smaller than the QMC value.¹¹ For higher spin, the mean field estimates, $J_{\perp c}[S = 1] \approx 6.095$ and $J_{\perp c}[S = 3/2] \approx 11.428$, are significantly smaller than our QMC results. This comparison is summarized in Table I. The scaling result $J_{\perp c} \sim S(S+1)$ has been suggested in Ref. 21 on the basis of series expansion calculations. Remarkably, as shown in Fig. 6, this scaling relation derived from mean-field theory seems to be reasonably accurate even for exact QMC results.

TABLE I. Value of $J_{\perp c}$ on the square lattice from different methods for different values of S . MFT stands for mean-field theory. The QMC data for $S = 1/2$ are from Ref. 11. The column ‘‘MFT+triplet interactions’’ gives variational results appropriate for $S = 1/2$. The column ‘‘MFT+quintet coupling’’ gives variational results appropriate for $S > 1/2$.

S	QMC	MFT	MFT + triplet interactions	MFT + quintet coupling
0.5	2.5220(1) ¹¹	2.287	2.568	
1	7.150(2)	6.098	6.387	7.32(14)
1.5	13.634(3)	11.434	11.714	13.32(1)

B. Honeycomb lattice bilayer

The honeycomb lattice is composed of two interpenetrating triangular lattices, as shown in Fig. 7. Operators, therefore, come with an additional sublattice index that distinguishes A and B sublattices. The mean-field Hamiltonian is given by

$$H_{\square}^{(0)} = -N_{\perp} J_{\perp} S(S+1) \bar{s}^2 - N_{\perp} \mu \bar{s}^2 + N_{\perp} \mu - \frac{3N_{\perp} C}{2} + \sum_{\mathbf{k}, u} \psi_{\mathbf{k}, u}^{\dagger} M_{\mathbf{k}} \psi_{\mathbf{k}, u}, \quad (15)$$

where $C = [J_{\perp} \{1 - S(S+1)\} - \mu]$. N_{\perp} denotes the number of interlayer bonds in the honeycomb bilayer. The operator $\psi_{\mathbf{k}, u}$ and the Hamiltonian matrix $M_{\mathbf{k}}$ are given by

$$\psi_{\mathbf{k}, u} = \begin{pmatrix} t_{\mathbf{k}, A, u} \\ t_{\mathbf{k}, B, u} \\ t_{-\mathbf{k}, A, u}^{\dagger} \\ t_{-\mathbf{k}, B, u}^{\dagger} \end{pmatrix}, \quad M_{\mathbf{k}} = \begin{pmatrix} C & \beta_{\mathbf{k}} & 0 & \beta_{\mathbf{k}} \\ \beta_{\mathbf{k}}^* & C & \beta_{\mathbf{k}}^* & 0 \\ 0 & \beta_{\mathbf{k}} & C & \beta_{\mathbf{k}} \\ \beta_{\mathbf{k}}^* & 0 & \beta_{\mathbf{k}}^* & C \end{pmatrix}, \quad (16)$$

where $\beta_{\mathbf{k}} = 2 \frac{S(S+1)}{3} \bar{s}^2 \gamma_{\mathbf{k}}$, with $\gamma_{\mathbf{k}} = 1 + e^{-ik_b} + e^{-ik_a - ik_b}$, and we have defined $k_a \equiv \mathbf{k} \cdot \hat{a}$ and $k_b \equiv \mathbf{k} \cdot \hat{b}$. Diagonalizing this Hamiltonian (see Appendix B), we obtain two eigenvalues for every \mathbf{k} . The eigenvalues are given by $\lambda_{\mathbf{k}, 1/2} = \sqrt{C^2 \mp 2C|\beta_{\mathbf{k}}|}$. The mean-field ground-state energy is given by

$$E_{\square}^{(0)} = -N_{\perp} J_{\perp} S(S+1) \bar{s}^2 - N_{\perp} \mu \bar{s}^2 + N_{\perp} \mu - \frac{3N_{\perp} C}{2} + 3 \sum_{\mathbf{k}} (\lambda_{\mathbf{k}, 1} + \lambda_{\mathbf{k}, 2}). \quad (17)$$

As before, we demand $\partial E_{\square}^{(0)} / \partial \mu = 0$ and $\partial E_{\square}^{(0)} / \partial \bar{s}^2 = 0$. This leads to the two mean-field equations

$$\bar{s}^2 = \frac{5}{2} - \frac{3}{N_{\perp}} \sum_{\mathbf{k}} \left[\frac{C - |\beta_{\mathbf{k}}|}{\lambda_{\mathbf{k}, 1}} + \frac{C + |\beta_{\mathbf{k}}|}{\lambda_{\mathbf{k}, 2}} \right], \quad (18)$$

$$\mu = -\frac{2CS(S+1)}{N_{\perp}} \sum_{\mathbf{k}} |\gamma_{\mathbf{k}}| \left[\frac{1}{\lambda_{\mathbf{k}, 1}} - \frac{1}{\lambda_{\mathbf{k}, 2}} \right] - J_{\perp} S(S+1). \quad (19)$$

Using the values of \bar{s} and μ thus obtained, we calculate the gap to triplet excitations. The dimer-Néel transition occurs when the triplon gap vanishes at $J_{\perp} = J_{\perp c}$. Using the above equations, we arrive at the following two results at the critical point. (i) The value \bar{s} at the dimer-Néel critical point is independent of spin and is given by

$$\bar{s}_c^2 = \frac{5}{2} + \frac{3}{2N_{\perp}} \sum_{\mathbf{k}} \left[\frac{|\gamma_{\mathbf{k}}| - 6}{\sqrt{9 - 3|\gamma_{\mathbf{k}}|}} - \frac{|\gamma_{\mathbf{k}}| + 6}{\sqrt{9 + 3|\gamma_{\mathbf{k}}|}} \right]. \quad (20)$$

A numerical evaluation shows $\bar{s}_c \approx 0.872$. (ii) We find the location of the dimer-Néel critical point

$$\frac{J_{\perp c}}{S(S+1)} = 10 - \frac{36}{N_{\perp}} \sum_{\mathbf{k}} \left[\frac{1}{\sqrt{9 - 3|\gamma_{\mathbf{k}}|}} + \frac{1}{\sqrt{9 + 3|\gamma_{\mathbf{k}}|}} \right]. \quad (21)$$

A numerical evaluation yields $J_{\perp c} \approx 1.748S(S+1)$. For $S = 1/2$, the mean-field result, $J_{\perp c}[S = 1/2] \approx 1.311$, is somewhat smaller than the QMC value. For higher spin, the

TABLE II. Value of $J_{\perp c}$ on the honeycomb lattice from different methods for different values of S . MFT stands for mean-field theory.

S	QMC	MFT	MFT + triplet interactions	MFT + quintet coupling
0.5	1.645(1)	1.312	1.588	
1	4.785(1)	3.498	3.774	4.80(9)
1.5	9.194(3)	6.559	6.837	9.58(18)

mean-field critical points, $J_{\perp c}[S = 1] \approx 3.496$ and $J_{\perp c}[S = 3/2] \approx 6.555$, are significantly smaller than the corresponding QMC results. This is summarized in Table II. Remarkably, as shown in Fig. 6, the scaling result $J_{\perp c} \sim S(S+1)$ from mean-field theory appears to be valid even for the exact QMC results on the honeycomb lattice. We have also explicitly checked that triplon condensation of the mode with energy $\lambda_{\mathbf{k}, 1}$ at momentum $\mathbf{k} = (0, 0)$ yields Néel order on the honeycomb bilayer.

V. BEYOND MEAN-FIELD THEORY: VARIATIONAL ANALYSIS

Corrections to the mean-field Hamiltonian arise from triplet-triplet interactions and coupling to higher spin objects such as quintets and heptets. As a function of S , we find two regimes where two different correction terms dominate. For $S = 1/2$, the only correction stems from triplet-triplet interactions since higher spin states are absent. For $S > 1/2$, the dominant correction arises from coupling to higher spin (quintet) states. Ordinarily, such quintet terms can be ignored as the energy cost of exciting quintets is large; however, these terms scale as S^2 as opposed to the S^0 scaling of the triplet-triplet interactions and they play an increasingly important role for larger S . These two correction terms are separately discussed in the following two sections.

Specifically, for the two regimes $S = 1/2$ and $S > 1/2$, we identify the leading correction term and take it into account using a variational approach. With the leading correction, the Hamiltonian takes the form $H_{\square}^{(0)} \rightarrow H_{\square}^{(0)} + \Delta H_{\square}$ and $H_{\square}^{(0)} \rightarrow H_{\square}^{(0)} + \Delta H_{\square}$. We treat ΔH as a perturbation acting upon the states of $H^{(0)}$. As a variational ansatz, we assume that the effect of the correction terms is entirely accounted for by a renormalization of the parameters \bar{s} and μ , which enter the mean-field Hamiltonian, $H_{\square}^{(0)}$ or $H_{\square}^{(0)}$. We choose μ to enforce single boson occupancy per site on average. The perturbations ΔH , for both regimes, preserve total boson number. Thus, it suffices to evaluate the total boson number using $H^{(0)}$. This gives us the constraint

$$\bar{s}^2 + \sum_{i, m} \langle t_{i, m}^{\dagger} t_{i, m} \rangle = N_{\perp}, \quad (22)$$

where the expectation value is evaluated with respect to $H^{(0)}$. (For the honeycomb lattice case, there is an additional sum over the sublattice degree of freedom in the above equation.) This leads precisely to the mean-field number constraint in Eq. (11) or Eq. (18), which can now be used to determine μ . The parameter \bar{s} is chosen to minimize the ground-state energy, evaluated to leading order in perturbation theory.

For $S = 1/2$, we find that the leading correction is obtained within first-order perturbation theory in ΔH . For $S > 1/2$, the dominant perturbing terms require us to go to second order in perturbation theory. In the next two sections, we discuss these correction terms in detail.

VI. TRIPLET INTERACTION CORRECTIONS

A. Triplet interactions on the square lattice

Staying within the singlet-triplet sector, the term we have ignored in the mean-field treatment is the triplet-triplet interaction term. For $S = 1/2$, there are no higher spin bosons beyond the singlet-triplet sector, so this is the only correction. For $S > 1/2$, this constitutes one term in a slew of correction terms. For any spin S , the triplet interaction terms are given by

$$\Delta H_{\square}^{(0)} = -\frac{1}{2} \sum_{(ij)} \sum_{\substack{u,v,w,v',w' \\ \in \{x,y,z\}}} \epsilon_{uvw} t_{i,v}^{\dagger} t_{i,w} \epsilon_{uv'w'} t_{j,v'}^{\dagger} t_{j,w'}. \quad (23)$$

We note that there are no cubic terms in triplet operators. As described in Ref. 33, this makes our bilayer problem qualitatively different from other dimerized states such as the spin-1/2 staggered dimer on the square lattice. Typically, triplet-triplet interactions such as those of Eq. (23) are taken into account within a self-consistent Hartree-Fock approximation.^{30,34} Here, we take the interactions in Eq. (23) to be a perturbation acting on $H_{\square}^{(0)}$ and evaluate the first-order correction to ground-state energy. To this end, we decouple $\Delta H_{\square}^{(0)}$ using bilinears that possess finite expectation values at the level of mean-field theory:

$$\begin{aligned} \langle t_{i,v}^{\dagger} t_{i+\delta,w} \rangle &\equiv \delta_{v,w} \rho, \\ \langle t_{i,v}^{\dagger} t_{i+\delta,w}^{\dagger} \rangle &\equiv \delta_{v,w} \Delta. \end{aligned} \quad (24)$$

Here, i and $i + \delta$ are nearest neighbors on the square lattice. Explicit expressions for ρ and Δ are given in Appendix A. We note that ρ and Δ are functions of the variational parameters \bar{s} and μ . The first-order energy correction due to triplet interactions is given by

$$\Delta E_{\square}^{(0)} = \langle \Delta H_{\square}^{(0)} \rangle = 6N_{\perp} [\rho^2 - \Delta^2]. \quad (25)$$

Thus, the variational energy of the ground state upon including the triplet interaction term is given by

$$E_{\square,\text{var}}^{(0)}(\bar{s}, \mu) = E_{\square}^{(0)} + \Delta E_{\square}^{(0)}, \quad (26)$$

where $E_{\square}^{(0)}$ is as defined in Eq. (10). The parameter \bar{s} is chosen to minimize this energy. We find that triplet interactions reduce the stability of the dimer phase and shift $J_{\perp c}$ to larger values. For $S = 1/2$, this leads to a renormalized transition point $J_{\perp c} \approx 2.58$, very close to the QMC result. For $S > 1/2$, the renormalization is too weak to account for the discrepancy between the earlier mean-field result and the QMC data. These triplet corrected results for the square lattice are summarized in Table I.

B. Triplet interactions on the honeycomb lattice

The interaction between triplets on the honeycomb lattice is given by

$$\begin{aligned} \Delta H_{\circlearrowleft}^{(0)} &= -\frac{1}{2} \sum_{i,\delta} \sum_{\substack{u,v,w,v',w' \\ \in \{x,y,z\}}} \epsilon_{uvw} t_{i,A,v}^{\dagger} t_{i,A,w} \\ &\times \epsilon_{uv'w'} t_{i+\delta,B,v'}^{\dagger} t_{i+\delta,B,w'}. \end{aligned} \quad (27)$$

The operators δ are such that the sites (i,A) and $(i+\delta,B)$ are nearest neighbors. This interaction term contributes to the ground-state energy at first order in perturbation theory. To evaluate this correction, we quadratically decompose the interaction using the following two bilinears:

$$\begin{aligned} \langle t_{i,A,v}^{\dagger} t_{i+\delta,B,w} \rangle &\equiv \delta_{v,w} \rho, \\ \langle t_{i,A,v}^{\dagger} t_{i+\delta,B,w}^{\dagger} \rangle &\equiv \delta_{v,w} \Delta, \end{aligned} \quad (28)$$

with the expectation values to be evaluated using the unperturbed Hamiltonian $H_{\circlearrowleft}^{(0)}$. Explicit expressions for ρ and Δ are given in Appendix B. The first-order correction to ground-state energy is given by

$$\Delta E_{\circlearrowleft}^{(0)} = \frac{9}{2} N_{\perp} [\rho^2 - \Delta^2]. \quad (29)$$

The parameter \bar{s} is chosen to minimize the energy,

$$E_{\circlearrowleft,\text{var}}^{(0)}(\bar{s}, \mu) = E_{\circlearrowleft}^{(0)} + \Delta E_{\circlearrowleft}^{(0)}. \quad (30)$$

As on the square lattice, we find that triplet interactions reduce the stability of the dimer phase and shift $J_{\perp c}$ to larger values. For $S = 1/2$, this leads to a renormalized transition point $J_{\perp c} \approx 1.59$, which is in reasonable agreement with the QMC result $J_{\perp c} = 1.645(1)$. For $S > 1/2$, however, the renormalization is again too weak to account for the QMC data. These triplet corrected results for the critical point on the honeycomb lattice are summarized in Table II.

VII. QUINTET CORRECTIONS

In the previous section, we have seen that triplet correction terms lead to a reasonably good agreement with QMC results for the dimer-Néel quantum critical point for $S = 1/2$. However, they fail to account for the significant discrepancy between QMC and bond operator mean-field theory for $S > 1/2$. This leads to us to suspect that higher-order spin excitations on the dimer bonds must be responsible for this difference. Upon including quintet terms, the spin operators at a site i contain a large number of terms as given in Eqs. (20) and (21) of Ref. 24 and reproduced in Appendix C for convenience.

Using these spin expressions to rewrite the Hamiltonian in Eq. (1), we find that correction terms beyond mean-field theory, including those involving quintet states, may be grouped as

$$\Delta H = \hat{D}_{tttt} + \bar{s} \hat{R}_{ttq}(S^2) + \hat{F}_{ttqq}(S^2) + \hat{G}_{qqqq}(S^0). \quad (31)$$

The subscripts indicate the composition of the terms in terms of bond operators. The scaling of each term with S is indicated in parentheses. For example, $\hat{R}_{ttq}(S^2)$ is composed of terms that involve two triplet operators and one quintet operator, and the coefficients of these terms scale as S^2 . The term that

we have accounted for in the previous section is \hat{D}_{ttt} , which scales as S^0 and contains four triplet operators. Naively, terms involving quintets should be less important due to the energy cost of exciting quintets. However, we see from the above classification of terms that the coefficients of $\hat{R}_{ttq}(S^2)$ and $\hat{F}_{ttq}(S^2)$ increase rapidly with increasing spin. We find that $\hat{R}_{ttq}(S^2)$ is, in fact, the dominant contribution for all $S > 1/2$. (For the case of $S = 1$, we have explicitly checked that this term dominates over triplet-triplet interactions encoded by \hat{D}_{ttt} ; see Table I.) The term $\hat{F}_{ttq}(S^2)$ is suppressed because it involves two quintet operators that act on different sites. In our variational scheme, this term will contribute to the ground-state energy at second order in perturbation theory. However, as the quintets are taken to be localized excitations, this term will involve intermediate states with two quintet excitations. Therefore, it will contribute much less than $\hat{R}_{ttq}(S^2)$.

In the vicinity of the dimer-Néel transition, we assert that $\hat{R}_{ttq}(S^2)$ will remain the dominant correction term for any $S > 1/2$ even if higher spin states such as heptets, nonets, etc., are included. As the dimer-Néel transition occurs via condensation of triplet excitations, it is reasonable that the dominant corrections come from quintets which are immediately higher in energy than triplets. Heptets, nonets, etc. occur at much higher energies and are unlikely to affect the triplet condensation point. To argue that this is indeed the case, we first note that the Hamiltonian of Eq. (1) can change the spin of a bond by ± 1 at most (this can be seen from the rotation properties of a single spin operator acting on a bond eigenstate). For example, if we restrict our attention to one particular bond, the Hamiltonian connects a triplet state to singlet, triplet, and quintet states. The matrix element connecting the triplet to a nonet state (or a state of even higher spin) is zero. Similarly, on a given bond, the heptet state has nonzero matrix elements only with quintet, heptet, and nonet states. The resulting terms in the Hamiltonian involving heptets, nonets, etc. will *not* contribute at second order in perturbation theory, but will only appear at higher order. As an illustration, upon including heptets, the Hamiltonian can have a term of the form $h_{i,m}^\dagger q_{i,n} t_{j,m}^\dagger t_{j,n'}$. Clearly, this term does not contribute to ground-state energy at first or second order. In addition, at whichever order it contributes, the energy denominators will involve large heptet excitation energies which will further suppress the energy contribution.

In summary, in the vicinity of the dimer-Néel transition for any value of $S > 1/2$, the leading correction to bond operator mean-field theory comes from $\bar{s} \hat{R}_{ttq}(S^2)$. We write

$$\Delta H^{(S>1/2)} \approx \Delta H^{(q)} \equiv \bar{s} \hat{R}_{ttq}(S^2). \quad (32)$$

Note that if we were to use a path-integral approach to integrate out the quintet excitations at this stage, we would be led to an *effective* triplet-triplet interaction which is enhanced by a factor of S^4 compared to the bare triplet-triplet term discussed in the previous section (although it would be divided by the quintet gap, which scales as S^2 near the Néel to dimer transition). Here we follow a different route, similar in spirit, and treat this term perturbatively assuming the quintet states to be local excitations. The energy cost of creating a quintet is given

by Eq. (3). We measure this energy cost from the Lagrange multiplier μ to get

$$\varepsilon_q - \mu = J_\perp \{3 - S(S+1)\} - \mu \quad (33)$$

as the energy cost of a quintet excitation.

A. Quintet corrections on the square lattice

The terms in $\bar{s} \hat{R}_{ttq}(S^2)$ may be organized as

$$\bar{s} \hat{R}_{ttq}(S^2) = \bar{s} \sum_i \sum_{n=-2, \dots, 2} \left[q_{i,n}^\dagger \sum_\delta \hat{T}_{i,i+\delta}^{[n]} + \text{H.c.} \right]. \quad (34)$$

The operator $\hat{T}_{i,i+\delta}^{[n]}$ is composed of triplet bilinears. The index δ sums over the four nearest-neighbor vectors on the square lattice. The explicit form of these operators is given in Appendix D. The operator $\hat{R}_{ttq}(S^2)$ does not contribute to ground-state energy at first order, as it is linear in quintet operators. The energy correction, at second order, is given by

$$\Delta E_\square^{(q)} = \bar{s}^2 \sum_{\sigma \neq 0} \sum_{\substack{i,n,\delta \\ i',n',\delta'}} \frac{\langle 0 | q_{i',n'} (\hat{T}_{i',i'+\delta'}^{[n]})^\dagger | \sigma \rangle \langle \sigma | q_{i,n} \hat{T}_{i,i+\delta}^{[n]} | 0 \rangle}{E_0 - E_\sigma}. \quad (35)$$

The index σ sums over all excited states of $H_\square^{(0)}$, the variational Hamiltonian. The only intermediate states that contribute are those with a single quintet. In our variational formalism, we take the quintets to be local excitations. This constrains us to ($i = i'$), ($n = n'$). This leaves us with

$$\Delta E_\square^{(q)} = \bar{s}^2 \sum_{v \neq 0} \sum_{i,n} \frac{\langle 0 | \sum_{\delta'} (\hat{T}_{i,i+\delta'}^{[n]})^\dagger | v \rangle \langle v | \sum_\delta \hat{T}_{i,i+\delta}^{[n]} | 0 \rangle}{E_0 - E_v}. \quad (36)$$

The intermediate states $|v\rangle$ which contribute involve a single quintet excitation. Within the triplet sector, at zero temperature, the intermediate states can have either (a) no triplon quasiparticles or (b) two triplon quasiparticles. The contribution from states with no triplon quasiparticles vanishes due to global spin-rotational symmetry of the Hamiltonian. The energy correction from two triplon intermediate states is evaluated to obtain the energy correction, $\Delta E_\square^{(q)}$. The complete expression is given in Appendix D.

Being second order in $\hat{R}_{ttq}(S^2)$, the energy correction from quintet coupling naively scales as S^4 for large S . However, the energy denominator involves the energy of quintet states, which is proportional to J_\perp . Close to the dimer-Néel transition, at the mean-field level, J_\perp approximately scales as S^2 for large S [see Eq. (14)]. We expect perturbative corrections to preserve this scaling of J_\perp with S^2 . Thus, near the dimer-Néel transition, $\Delta E_\square^{(q)}$ scales as $S^4/S^2 \sim S^2$. The ground-state energy to leading order in perturbation theory is thus given by

$$E_{\square, \text{var}}^{(S>1/2)}(\bar{s}, \mu) = E_\square^{(0)} + \Delta E_\square^{(q)}. \quad (37)$$

This energy is a function of \bar{s} and μ . As discussed earlier, μ is tuned to enforce single boson occupancy per site, while \bar{s} is chosen to minimize $E_{\square, \text{var}}^{(S>1/2)}(\bar{s}, \mu)$.

Having determined \bar{s} and μ variationally, we can find the gap to triplon excitations as a function of J_{\perp} . The dimer-Néel transition is indicated by the vanishing of the triplon gap in the variationally obtained state. As summarized in Table I, the renormalized critical points obtained in this manner are within 2.5% of the QMC results. While the precise quantitative agreement is perhaps fortuitous, and will certainly change depending on the nature of the approximations made, the important problem we have resolved is to show that the large discrepancy between QMC and simple bond operator mean-field theory for $S > 1/2$ can be accounted for by virtual quintet excitations.

B. Quintet corrections on the honeycomb lattice

On the honeycomb lattice, the terms in $\bar{s}\hat{R}_{ttq}(S^2)$ may be written as

$$\bar{s}\hat{R}_{ttq} = \bar{s} \sum_i \sum_{n=-2, \dots, 2} \left[q_{i,A,n}^{\dagger} \sum_{\delta} \hat{A}_{i,i+\delta}^{[n]} + \text{H.c.} + q_{i,B,n}^{\dagger} \sum_{\delta} \hat{B}_{i,i-\delta}^{[n]} + \text{H.c.} \right]. \quad (38)$$

The operators $\hat{A}_{i,i+\delta}$ and $\hat{B}_{i,i-\delta}$ are triplet bilinears centered on nearest-neighbor bonds. We give their explicit forms in momentum space in Appendix E. The terms in $\hat{R}_{ttq}(S^2)$ contribute to ground-state energy only at second order in perturbation theory. The energy correction may be written as

$$\Delta E_{\square}^{(q)} = \bar{s}^2 \sum_{\sigma \neq 0} \sum_{i,n} \langle 0 | \left[q_{i,A,n} \sum_{\delta'} \hat{A}_{i,i+\delta'}^{[n]} \right] | \sigma \rangle \times \langle \sigma | \left[q_{i,A,n}^{\dagger} \sum_{\delta} \hat{A}_{i,i+\delta}^{[n]} \right] | 0 \rangle / \{E_0 - E_{\sigma}\} + (A \rightarrow B), \quad (39)$$

where the index σ sums over all excited states of $H_{\square}^{(0)}$. As the terms in $\hat{R}_{ttq}(S^2)$ involve one quintet operator, only intermediate states with a single occupied quintet state will contribute,

$$\Delta E_{\square}^{(q)} = \bar{s}^2 \sum_{v \neq 0} \sum_{i,n} \frac{\langle 0 | \sum_{\delta'} (\hat{A}_{i,i+\delta'}^{[n]})^{\dagger} | v \rangle \langle v | \sum_{\delta} \hat{A}_{i,i+\delta}^{[n]} | 0 \rangle}{\{E_0 - E_v\}} + \bar{s}^2 \sum_{v \neq 0} \sum_{i,n} \frac{\langle 0 | \sum_{\delta'} (\hat{B}_{i,i-\delta'}^{[n]})^{\dagger} | v \rangle \langle v | \sum_{\delta} \hat{B}_{i,i-\delta}^{[n]} | 0 \rangle}{\{E_0 - E_v\}}. \quad (40)$$

We evaluate these overlaps in momentum space, as described in Appendix E. The intermediate state $|v\rangle$ could have either (i) no triplon quasiparticles or (ii) two triplon quasiparticles. However, the contribution from states with no triplons vanishes due to global spin rotational symmetry. The explicit expression for $\Delta E_{\square}^{(q)}$ is given in Appendix E. Thus, the energy of the ground state to leading order in quintet coupling is given by

$$E_{\square, \text{var}}^{(S>1/2)} = E_{\square}^{(0)} + \Delta E_{\square}^{(q)}. \quad (41)$$

We choose \bar{s} to minimize this energy. The vanishing of the triplet gap in the variationally determined state signals the dimer-Néel transition. Our results for $J_{\perp c}$ on the honeycomb lattice are shown in Table II. The renormalized critical points for $S = 1$ and $3/2$ are within 5% of the QMC value.

VIII. DISCUSSION

In this paper, we have studied the Néel to dimer transition in Heisenberg antiferromagnets on bilayer square and honeycomb lattices for different spin values using QMC and bond operator approaches. The critical bilayer exchange $J_{\perp c}$ scales as $S(S+1)$ within both bond operator mean-field theory and QMC simulations. However, there is a systematic deviation between bond operator mean-field theory and QMC, with the deviation itself scaling as $\sim S^2$. Our variational extension of bond operator theory to include the dominant triplet and quintet excitations successfully captures this systematic deviation and gives a more precise estimate of $J_{\perp c}$.

$\text{Bi}_3\text{Mn}_4\text{O}_{12}(\text{NO}_3)$ provides an example of a bilayer honeycomb antiferromagnet²⁵ with $S = 3/2$, where strong interlayer exchange couplings $\sim 2J_1$ have been inferred from electronic structure calculations.³⁵ Despite this strong bilayer coupling, our study indicates that this material would be deep in the Néel ordered phase if there are no other frustrating interactions. We are thus forced to attribute the observed lack of magnetic order in $\text{Bi}_3\text{Mn}_4\text{O}_{12}(\text{NO}_3)$ to frustration effects arising from further neighbor couplings; such further neighbor interactions have been shown to drive a variety of new phases on the honeycomb lattice.^{36–43} One recent example of a dimer system with $S = 1$ is the triangular dimer material^{13,44} $\text{Ba}_3\text{Mn}_2\text{O}_8$. Our approach could be applied to understand the triplon spectrum and the effect of quintet corrections in this material. In particular, our work shows that extracting exchange couplings from fitting experimental data to bond operator mean-field theory may not yield precise estimates. In summary, our work provides a starting point to think about the physics of high-spin Heisenberg antiferromagnets in a variety of model systems and materials.

ACKNOWLEDGMENTS

This research was supported by the Canadian NSERC (R.G., A.P.), an Ontario Early Researcher Award (R.G., A.P.), and the Swiss HP²C initiative (SVI). The quantum Monte Carlo simulations were performed on the Brutus cluster at ETH Zurich. RG thanks J. Rau, V. Vijay Shankar and C. M. Puetter for discussions.

APPENDIX A: SQUARE BILAYER: BOSONIC BOGOLIUBOV TRANSFORMATION

The MFT Hamiltonian of Eq. (7) is diagonalized by a pseudounitary matrix,

$$U_{\mathbf{k}} = \begin{pmatrix} \cosh \theta_{\mathbf{k}} & \sinh \theta_{\mathbf{k}} \\ \sinh \theta_{\mathbf{k}} & \cosh \theta_{\mathbf{k}} \end{pmatrix}. \quad (A1)$$

Imposing $\tanh 2\theta_{\mathbf{k}} = -2\epsilon_{\mathbf{k}}/(A + 2\epsilon_{\mathbf{k}})$, we get

$$\psi_{\mathbf{k},u}^{\dagger} \begin{pmatrix} A + 2\epsilon_{\mathbf{k}} & 2\epsilon_{\mathbf{k}} \\ 2\epsilon_{\mathbf{k}} & A + 2\epsilon_{\mathbf{k}} \end{pmatrix} \psi_{\mathbf{k},u} = \phi_{\mathbf{k},u}^{\dagger} \begin{pmatrix} \lambda_{\mathbf{k}} & 0 \\ 0 & \lambda_{\mathbf{k}} \end{pmatrix} \phi_{\mathbf{k},u}. \quad (A2)$$

We have defined new quasiparticle operators given by $\psi_{\mathbf{k},u} = U_{\mathbf{k}}\phi_{\mathbf{k},u}$ so that

$$\begin{pmatrix} t_{\mathbf{k},u} \\ t_{-\mathbf{k},u}^\dagger \end{pmatrix} = \begin{pmatrix} \cosh \theta_{\mathbf{k}} & \sinh \theta_{\mathbf{k}} \\ \sinh \theta_{\mathbf{k}} & \cosh \theta_{\mathbf{k}} \end{pmatrix} \begin{pmatrix} \tau_{\mathbf{k},u} \\ \tau_{-\mathbf{k},u}^\dagger \end{pmatrix}. \quad (\text{A3})$$

The τ operators are the triplon quasiparticles. The bilinears defined in Eq. (24) may be evaluated using the elements of U as follows:

$$\begin{aligned} \rho &= \frac{1}{4N_{\perp}} \sum_{\mathbf{k},\delta} [\langle t_{\mathbf{k},v}^\dagger t_{\mathbf{k},v} \rangle e^{i\mathbf{k}\cdot\delta}] \\ &= \frac{1}{4N_{\perp}} \sum_{\mathbf{k}}' (2 \cos k_x + 2 \cos k_y) \frac{A + 2\epsilon_{\mathbf{k}}}{\lambda_{\mathbf{k}}}, \quad (\text{A4}) \end{aligned}$$

$$\begin{aligned} \Delta &= \frac{1}{4N_{\perp}} \sum_{\mathbf{k},\delta} [\langle t_{\mathbf{k},v}^\dagger t_{-\mathbf{k},v}^\dagger \rangle e^{i\mathbf{k}\cdot\delta}] \\ &= \frac{1}{4N_{\perp}} \sum_{\mathbf{k}}' (2 \cos k_x + 2 \cos k_y) \frac{(-2\epsilon_{\mathbf{k}})}{\lambda_{\mathbf{k}}}. \quad (\text{A5}) \end{aligned}$$

APPENDIX B: HONEYCOMB BILAYER: BOSONIC BOGOLIUBOV TRANSFORMATION

The mean-field Hamiltonian of Eq. (15) may be diagonalized by the matrix

$$P_{\mathbf{k}} = \frac{1}{\sqrt{2}} \begin{pmatrix} 1 & 1 & 0 & 0 \\ -b_{\mathbf{k}} & b_{\mathbf{k}} & 0 & 0 \\ 0 & 0 & 1 & 1 \\ 0 & 0 & -b_{\mathbf{k}} & b_{\mathbf{k}} \end{pmatrix} \begin{pmatrix} C_{\mathbf{k},1} & 0 & S_{\mathbf{k},1} & 0 \\ 0 & C_{\mathbf{k},2} & 0 & S_{\mathbf{k},2} \\ S_{\mathbf{k},1} & 0 & C_{\mathbf{k},1} & 0 \\ 0 & S_{\mathbf{k},2} & 0 & C_{\mathbf{k},2} \end{pmatrix}.$$

Here, we have defined $b_{\mathbf{k}} \equiv \beta_{\mathbf{k}}^*/|\beta_{\mathbf{k}}|$. We take the other entries to be hyperbolic functions given by $C_{\mathbf{k},n} = \cosh \kappa_{\mathbf{k},n}$ and $S_{\mathbf{k},n} = \sinh \kappa_{\mathbf{k},n}$, with $n = 1, 2$. With this definition, this matrix $P_{\mathbf{k}}$ satisfies the pseudounitariness condition $P_{\mathbf{k}}\sigma P_{\mathbf{k}}^\dagger = \sigma$, where $\sigma = \text{diag}\{1, 1, -1, -1\}$. To diagonalize the Hamiltonian matrix $M_{\mathbf{k}}$, we set

$$\begin{aligned} \tanh 2\kappa_{\mathbf{k},1} &= \beta_{\mathbf{k}}/(C - \beta_{\mathbf{k}}), \\ \tanh 2\kappa_{\mathbf{k},2} &= -\beta_{\mathbf{k}}/(C + \beta_{\mathbf{k}}). \end{aligned} \quad (\text{B1})$$

With this choice, the matrix $P_{\mathbf{k}}$ diagonalizes the Hamiltonian,

$$P_{\mathbf{k}}^\dagger M_{\mathbf{k}} P_{\mathbf{k}} = \text{diag}\{\lambda_{\mathbf{k},1}, \lambda_{\mathbf{k},2}, \lambda_{\mathbf{k},1}, \lambda_{\mathbf{k},2}\}, \quad (\text{B2})$$

where $\lambda_{\mathbf{k},1/2}$ are as defined in the body of the text. We transform the triplet operators defined in Eq. (16) into new quasiparticle operators using

$$\begin{pmatrix} t_{\mathbf{k},A,u} \\ t_{\mathbf{k},B,u} \\ t_{-\mathbf{k},A,u}^\dagger \\ t_{-\mathbf{k},B,u}^\dagger \end{pmatrix} = P_{\mathbf{k}} \begin{pmatrix} \vartheta_{\mathbf{k},1,u} \\ \vartheta_{\mathbf{k},2,u} \\ \vartheta_{-\mathbf{k},1,u}^\dagger \\ \vartheta_{-\mathbf{k},2,u}^\dagger \end{pmatrix}. \quad (\text{B3})$$

The ϑ operators are the triplon quasiparticles. Compared to the square lattice case, the quasiparticle operators have an additional index on account of the sublattice degree of freedom. We can express our original triplet operators as

follows:

$$\begin{aligned} t_{\mathbf{k},A,u} &= \sum_{f=1,2} (C_{\mathbf{k},f} \vartheta_{\mathbf{k},f,u} + S_{\mathbf{k},f} \vartheta_{-\mathbf{k},f,u}^\dagger), \\ t_{-\mathbf{k},B,u} &= \sum_{f=1,2} (-1)^f b_{\mathbf{k}}^* (C_{\mathbf{k},f} \vartheta_{-\mathbf{k},f,u} + S_{\mathbf{k},f} \vartheta_{\mathbf{k},f,u}^\dagger). \end{aligned} \quad (\text{B4})$$

The bilinears defined in Eq. (28) can be evaluated as

$$\begin{aligned} \rho &= \frac{2}{3N_{\perp}} \sum_{\mathbf{k}} \langle t_{\mathbf{k},A,v}^\dagger t_{\mathbf{k},B,v} \rangle \gamma_{\mathbf{k}} \\ &= \frac{1}{6N_{\perp}} \sum_{\mathbf{k}} |\gamma_{\mathbf{k}}| \left[-\frac{C - |\beta_{\mathbf{k}}|}{\lambda_{\mathbf{k},1}} + \frac{C + |\beta_{\mathbf{k}}|}{\lambda_{\mathbf{k},2}} \right], \quad (\text{B5}) \\ \Delta &= \frac{2}{3N_{\perp}} \sum_{\mathbf{k}} \langle t_{\mathbf{k},A,v}^\dagger t_{-\mathbf{k},B,v}^\dagger \rangle \gamma_{\mathbf{k}} \\ &= \frac{-1}{6N_{\perp}} \sum_{\mathbf{k}} |\gamma_{\mathbf{k}}| \left[\frac{|\beta_{\mathbf{k}}|}{\lambda_{\mathbf{k},1}} + \frac{|\beta_{\mathbf{k}}|}{\lambda_{\mathbf{k},2}} \right]. \quad (\text{B6}) \end{aligned}$$

APPENDIX C: SPIN OPERATOR EXPRESSIONS INCLUDING QUINTET TERMS

Including triplet and quintet operators, the complete expression for the spin operators on the two layers of the bilayer are²⁴

$$\begin{aligned} S_{i,\ell=1,2}^+ &= (-1)^\ell \sqrt{\frac{2S(S+1)}{3}} \bar{s}(t_{i,-1} - t_{i,1}^\dagger) \\ &\quad + (-1)^\ell \sqrt{\frac{(2S-1)(2S+3)}{5}} \left[(t_{i,-1}^\dagger q_{i,-2} - q_{i,2}^\dagger t_{i,1}) \right. \\ &\quad \left. + \sqrt{\frac{1}{2}} (t_{i,0}^\dagger q_{i,-1} - q_{i,1}^\dagger t_{i,0}) + \sqrt{\frac{1}{6}} (t_{i,1}^\dagger q_{i,0} - q_{i,0}^\dagger t_{i,-1}) \right] \\ &\quad + \sqrt{\frac{1}{2}} (t_{i,1}^\dagger t_{i,0} + t_{i,0}^\dagger t_{i,-1}) + \sqrt{\frac{3}{2}} (q_{i,1}^\dagger q_{i,0} + q_{i,0}^\dagger q_{i,-1}) \\ &\quad + q_{i,2}^\dagger q_{i,1} + q_{i,-1}^\dagger q_{i,-2}, \quad (\text{C1}) \end{aligned}$$

with $S_{i,\ell=1,2}^-$ being its Hermitian conjugate, while

$$\begin{aligned} S_{i,\ell=1,2}^z &= (-1)^\ell \sqrt{\frac{S(S+1)}{3}} \bar{s}(t_{i,0} + t_{i,0}^\dagger) \\ &\quad + (-1)^\ell \sqrt{\frac{(2S-1)(2S+3)}{5}} \left[\sqrt{\frac{1}{3}} (t_{i,0}^\dagger q_{i,0} + q_{i,0}^\dagger t_{i,0}) \right. \\ &\quad \left. + \frac{1}{2} (t_{i,1}^\dagger q_{i,1} + q_{i,1}^\dagger t_{i,1} + t_{i,-1}^\dagger q_{i,-1} + q_{i,-1}^\dagger t_{i,-1}) \right] \\ &\quad + \frac{1}{2} (t_{i,1}^\dagger t_{i,1} - t_{i,-1}^\dagger t_{i,-1} + q_{i,1}^\dagger q_{i,1} - q_{i,-1}^\dagger q_{i,-1}) \\ &\quad + q_{i,2}^\dagger q_{i,2} - q_{i,-2}^\dagger q_{i,-2}. \quad (\text{C2}) \end{aligned}$$

APPENDIX D: SQUARE BILAYER: INCLUSION OF QUINTETS

Using the spin operators in Eq. (C1) and (C2), we now give explicit expressions for $\hat{R}_{i\ell q}(S^2)$. In the main text, we defined $\hat{R}_{i\ell q}(S^2)$ in terms of triplet bilinears $\hat{T}_{i,i+\delta}^{[n]}$. Here, we

give expressions for $\hat{T}_{i,i+\delta}^{[n]}$ in momentum space. We use the Fourier transform convention

$$t_{i,u \in \{x,y,z\}} = \frac{1}{\sqrt{N_{\perp}}} \sum_{\mathbf{k}} t_{\mathbf{k},u} e^{i\mathbf{k} \cdot \mathbf{r}_i}. \quad (\text{D1})$$

The operator $\hat{T}_{i,i+\delta}^{[n]}$ is composed of bilinears of the form $t_{i,u}(t_{i+\delta,v} \pm t_{i+\delta,v}^{\dagger})$. Using the Fourier transform, this generic bilinear may be written as $(1/N_{\perp}) \sum_{\mathbf{k},\mathbf{p}} t_{-\mathbf{k}+\mathbf{p},u}(t_{\mathbf{k},u} \pm t_{-\mathbf{k},u}^{\dagger}) e^{i\mathbf{k} \cdot \delta} e^{i\mathbf{p} \cdot \mathbf{r}_i}$.

Thus, we may write

$$\sum_{\delta} \hat{T}_{i,i+\delta}^{[n]} = \frac{M}{N_{\perp}} \sum_{\mathbf{k},\mathbf{p}} \hat{T}_{-\mathbf{k}+\mathbf{p},\mathbf{k}}^{[n]} e^{i\mathbf{p} \cdot \mathbf{r}_i} \eta_{\mathbf{k}}, \quad (\text{D2})$$

where $\eta_{\mathbf{k}} = \sum_{\delta} e^{i\mathbf{k} \cdot \delta} = 2(\cos k_x + \cos k_y)$ and the coefficient $M = \sqrt{\frac{S(S+1)(2S-1)(2S+3)}{30}}$. The explicit forms of $\hat{T}_{-\mathbf{k}+\mathbf{p},\mathbf{k}}^{[n]}$ are

$$\begin{aligned} \hat{T}_{-\mathbf{k}+\mathbf{p},\mathbf{k}}^{[-2]} &= \tilde{t}_{-\mathbf{k}+\mathbf{p},x}(t_{\mathbf{k},x} + t_{-\mathbf{k},x}^{\dagger}) - \tilde{t}_{-\mathbf{k}+\mathbf{p},y}(t_{\mathbf{k},y} + t_{-\mathbf{k},y}^{\dagger}) \\ &\quad + i\tilde{t}_{-\mathbf{k}+\mathbf{p},x}(t_{\mathbf{k},y} + t_{-\mathbf{k},y}^{\dagger}) + i\tilde{t}_{-\mathbf{k}+\mathbf{p},y}(t_{\mathbf{k},x} + t_{-\mathbf{k},x}^{\dagger}), \\ \hat{T}_{-\mathbf{k}+\mathbf{p},\mathbf{k}}^{[-1]} &= \tilde{t}_{-\mathbf{k}+\mathbf{p},z}(t_{\mathbf{k},x} + t_{-\mathbf{k},x}^{\dagger}) + \tilde{t}_{-\mathbf{k}+\mathbf{p},x}(t_{\mathbf{k},z} + t_{-\mathbf{k},z}^{\dagger}) \\ &\quad + i\tilde{t}_{-\mathbf{k}+\mathbf{p},z}(t_{\mathbf{k},y} + t_{-\mathbf{k},y}^{\dagger}) + i\tilde{t}_{-\mathbf{k}+\mathbf{p},y}(t_{\mathbf{k},z} + t_{-\mathbf{k},z}^{\dagger}), \\ \hat{T}_{-\mathbf{k}+\mathbf{p},\mathbf{k}}^{[0]} &= \sqrt{\frac{2}{3}} [-\tilde{t}_{-\mathbf{k}+\mathbf{p},x}(t_{\mathbf{k},x} + t_{-\mathbf{k},x}^{\dagger}) \\ &\quad - \tilde{t}_{-\mathbf{k}+\mathbf{p},y}(t_{\mathbf{k},y} + t_{-\mathbf{k},y}^{\dagger}) + 2\tilde{t}_{-\mathbf{k}+\mathbf{p},z}(t_{\mathbf{k},z} + t_{-\mathbf{k},z}^{\dagger})], \\ \hat{T}_{-\mathbf{k}+\mathbf{p},\mathbf{k}}^{[-1]} &= -\tilde{t}_{-\mathbf{k}+\mathbf{p},z}(t_{\mathbf{k},x} + t_{-\mathbf{k},x}^{\dagger}) - \tilde{t}_{-\mathbf{k}+\mathbf{p},x}(t_{\mathbf{k},z} + t_{-\mathbf{k},z}^{\dagger}) \\ &\quad + i\tilde{t}_{-\mathbf{k}+\mathbf{p},z}(t_{\mathbf{k},y} + t_{-\mathbf{k},y}^{\dagger}) + i\tilde{t}_{-\mathbf{k}+\mathbf{p},y}(t_{\mathbf{k},z} + t_{-\mathbf{k},z}^{\dagger}), \\ \hat{T}_{-\mathbf{k}+\mathbf{p},\mathbf{k}}^{[2]} &= \tilde{t}_{-\mathbf{k}+\mathbf{p},x}(t_{\mathbf{k},x} + t_{-\mathbf{k},x}^{\dagger}) - \tilde{t}_{-\mathbf{k}+\mathbf{p},y}(t_{\mathbf{k},y} + t_{-\mathbf{k},y}^{\dagger}) \\ &\quad - i\tilde{t}_{-\mathbf{k}+\mathbf{p},x}(t_{\mathbf{k},y} + t_{-\mathbf{k},y}^{\dagger}) - i\tilde{t}_{-\mathbf{k}+\mathbf{p},y}(t_{\mathbf{k},x} + t_{-\mathbf{k},x}^{\dagger}). \end{aligned} \quad (\text{D3})$$

$$E_{\mathbf{p}} = -2 \sum_{\mathbf{q}} \frac{[\sinh^2(\theta_{\mathbf{q}}) \eta_{\mathbf{p}-\mathbf{q}}^2 \{\cosh(2\theta_{\mathbf{p}-\mathbf{q}}) + \sinh(2\theta_{\mathbf{p}-\mathbf{q}})\} + \sinh^2(\theta_{\mathbf{p}-\mathbf{q}}) \eta_{\mathbf{q}}^2 \{\cosh(2\theta_{\mathbf{q}}) + \sinh(2\theta_{\mathbf{q}})\}]}{\varepsilon_{\mathbf{q}} - \mu + \lambda_{-\mathbf{q}} + \lambda_{-\mathbf{p}+\mathbf{q}}}. \quad (\text{D8})$$

APPENDIX E: HONEYCOMB BILAYER: INCLUSION OF QUINTETS

In the main text, we defined $\hat{R}_{ttq}(S^2)$ in terms of triplet bilinears $\hat{A}_{i,i+\delta}^{[n]}$ and $\hat{B}_{i-\delta,i}^{[n]}$. Here, we give expressions for $\hat{A}_{i,i+\delta}^{[n]}$ and $\hat{B}_{i-\delta,i}^{[n]}$ in momentum space. We use the Fourier transform convention

$$t_{i,\alpha \in \{A,B\}, u \in \{x,y,z\}} = \frac{1}{\sqrt{N_{\perp}/2}} \sum_{\mathbf{k}} t_{\alpha,\mathbf{k},u} e^{i\mathbf{k} \cdot \mathbf{r}_i}. \quad (\text{E1})$$

(i) The terms in $\hat{A}_{i,i+\delta}^{[n]}$ are of the form $t_{i,A,u}(t_{i+\delta,B,v} + t_{i+\delta,B,v}^{\dagger})$. Using our Fourier transform convention, we may write

$$\sum_{\delta} \hat{A}_{i,i+\delta}^{[n]} = \frac{M}{N_{\perp}/2} \sum_{\mathbf{k},\mathbf{p}} \hat{A}_{-\mathbf{k}+\mathbf{p},\mathbf{k}}^{[n]} e^{i\mathbf{p} \cdot \mathbf{r}_i} \gamma_{\mathbf{k}}, \quad (\text{E2})$$

We have denoted some triplet operators as t and some as \tilde{t} . For the purposes of the square lattice, this distinction can be ignored. We will use these same expressions in the context of the honeycomb lattice also. For the honeycomb case, t and \tilde{t} operators will act on different sublattices.

The energy correction due to coupling to quintets is given in Eq. (36). Using the Fourier transformed expression in Eq. (D2), we rewrite the energy as

$$\Delta E_{\square}^{S>1/2} = \frac{M^2 \bar{s}^2}{N_{\perp}} \sum_{m=-2,\dots,2} \sum_{\mathbf{p}} E_{\mathbf{p}}^{[m]}, \quad (\text{D4})$$

where \mathbf{p} is the momentum of the intermediate state. The quantity $E_{\mathbf{p}}^{[m]}$ is given by

$$E_{\mathbf{p}}^{[m]} = \sum_{v \neq 0} \frac{|\langle v | \sum_{\mathbf{k}} \hat{T}_{-\mathbf{k}+\mathbf{p},\mathbf{k}}^{[n]} \eta_{\mathbf{k}} | 0 \rangle|^2}{E_0 - E_v}. \quad (\text{D5})$$

Here, $(-\mathbf{p})$ is the momentum of the intermediate state $|v\rangle$. As described in Sec. VII A, the intermediate states $|v\rangle$ that contribute have two triplon quasiparticle excitations and one quintet excitation. In the triplet sector, an intermediate state with momentum $(-\mathbf{p})$ may be represented as

$$|v_{\text{two triplon}}\rangle = \tau_{\mathbf{q}-\mathbf{p},u}^{\dagger} \tau_{-\mathbf{q},v'}^{\dagger} |0\rangle. \quad (\text{D6})$$

With this parametrization, the sum over intermediate states $|v\rangle$ may be written as

$$\sum_{v \neq 0} \rightarrow \sum_{\mathbf{q}} \sum_{u',v' \in \{x,y,z\}}. \quad (\text{D7})$$

Evaluating the matrix elements using this parametrization of the intermediate state, we find that the energy contribution $E_{\mathbf{p}}^{[m]}$ is the same from every m sector, i.e., $E_{\mathbf{p}}^{[m]} = E_{\mathbf{p}}$ for all m . The quantity $E_{\mathbf{p}}$ is given by

where $\gamma_{\mathbf{k}} = \sum_{\delta} e^{i\mathbf{k} \cdot \delta} = 1 + e^{-ik_b} + e^{-ik_a - ik_b}$ and the coefficient $M = \sqrt{\frac{S(S+1)(2S-1)(2S+3)}{30}}$ is the same as that defined for the square lattice case. The explicit forms of $\hat{A}_{-\mathbf{k}+\mathbf{p},\mathbf{k}}^{[n]}$ are the same of those of $\hat{T}_{-\mathbf{k}+\mathbf{p},\mathbf{k}}^{[n]}$ given in Eq. (D3) with the following redefinition:

$$\tilde{t}_{\mathbf{k},u} \equiv t_{A,\mathbf{k},u}, \quad t_{\mathbf{k},u} \equiv t_{B,\mathbf{k},u}. \quad (\text{E3})$$

(ii) The terms in $\hat{B}_{i,i-\delta}^{[n]}$ are of the form $t_{i,B,u}(t_{i-\delta,A,v} \pm t_{i-\delta,A,v}^{\dagger})$. Using our Fourier transform convention, we write

$$\sum_{\delta} \hat{B}_{i,i-\delta}^{[n]} = \frac{M}{N_{\perp}/2} \sum_{\mathbf{k},\mathbf{p}} \hat{B}_{-\mathbf{k}+\mathbf{p},\mathbf{k}}^{[n]} e^{i\mathbf{p} \cdot \mathbf{r}_i} \gamma_{-\mathbf{k}}. \quad (\text{E4})$$

Explicit expressions for $\hat{B}_{-\mathbf{k}+\mathbf{p},\mathbf{k}}^{[m]}$ are the same as those of $\hat{T}_{-\mathbf{k}+\mathbf{p},\mathbf{k}}^{[m]}$ given in Eq. (D3) but with the following redefinition:

$$\tilde{t}_{\mathbf{k},u} \equiv t_{B,\mathbf{k},u}, \quad t_{\mathbf{k},u} \equiv t_{A,\mathbf{k},u}. \quad (\text{E5})$$

The quintet energy correction on the honeycomb lattice may be rewritten as

$$\Delta E^{(q)} = \frac{M^2 \bar{s}^2}{N_{\perp}/2} \sum_{\mathbf{p}} \sum_m [(A_{\mathbf{p}}^{[m]}) + (B_{\mathbf{p}}^{[m]})], \quad (\text{E6})$$

where

$$(A_{\mathbf{p}}^{[m]}) = \sum_{v \neq 0} \frac{|\langle v | \sum_{\mathbf{k}} \hat{A}_{-\mathbf{k}+\mathbf{p},\mathbf{k}}^{[m]} \gamma_{\mathbf{k}} | 0 \rangle|^2}{E_0 - E_v}, \quad (\text{E7})$$

$$(B_{\mathbf{p}}^{[m]}) = \sum_{v \neq 0} \frac{|\langle v | \sum_{\mathbf{k}} \hat{B}_{-\mathbf{k}+\mathbf{p},\mathbf{k}}^{[m]} \gamma_{-\mathbf{k}} | 0 \rangle|^2}{E_0 - E_v}.$$

The only intermediate states $|v\rangle$ that contribute to the energy are states with two triplon quasiparticle excitations. A generic intermediate state with momentum $(-\mathbf{p})$ may be characterized as

$$|v_{\text{two triplon}}\rangle = \vartheta_{-\mathbf{q},f,u}^{\dagger} \vartheta_{\mathbf{q}-\mathbf{p},g,v}^{\dagger} |0\rangle. \quad (\text{E8})$$

Using this parametrization of a generic state, the sum over intermediate states in Eq. (E7) becomes

$$\sum_{v \neq 0} \longrightarrow \frac{1}{2} \sum_{\mathbf{q}} \sum_{f,g \in \{1,2\}} \sum_{u,v \in \{x,y,z\}}. \quad (\text{E9})$$

There is a factor of 1/2 to account for double counting as $(\mathbf{q}' = \mathbf{p} - \mathbf{q}, f' = g, g' = f)$ corresponds to the same state as (\mathbf{q}, f, g) . Evaluating the necessary overlaps, we find that the contribution from each m is the same, $(A_{\mathbf{p}}^{[m]}) = (B_{\mathbf{p}}^{[m]}) = E_{\mathbf{p}}$ for $m = -2, \dots, 2$. The quantity $E_{\mathbf{p}}$ is given by

$$E_{\mathbf{p}} = -2 \sum_{\mathbf{q},f,g} \frac{[S_{\mathbf{q},f}(-1)^g (S_{-\mathbf{p}+\mathbf{q},g} + C_{\mathbf{p}-\mathbf{q},g}) |\gamma_{\mathbf{p}-\mathbf{q}}| + S_{\mathbf{p}-\mathbf{q},g}(-1)^f (S_{-\mathbf{q},f} + C_{\mathbf{q},f}) |\gamma_{\mathbf{q}}|]^2}{\varepsilon_{\mathbf{q}} - \mu + \lambda_{-\mathbf{q},f} + \lambda_{\mathbf{q}-\mathbf{p},g}}. \quad (\text{E10})$$

By plugging these expressions into Eq. (E6), the correction to ground-state energy may be computed.

¹T. Nikuni, M. Oshikawa, A. Oosawa, and H. Tanaka, *Phys. Rev. Lett.* **84**, 5868 (2000).

²T. M. Rice, *Science* **298**, 760 (2002).

³S. Sachdev, *Quantum Phase Transitions* (Cambridge University Press, Cambridge, 2001).

⁴T. Giamarchi, C. Rüegg, and O. Tchernyshyov, *Nat. Phys.* **4**, 198 (2008).

⁵A. Oosawa, M. Ishii, and H. Tanaka, *J. Phys. Condens. Matter* **11**, 265 (1999).

⁶M. Jaime, V. F. Correa, N. Harrison, C. D. Batista, N. Kawashima, Y. Kazuma, G. A. Jorge, R. Stein, I. Heinmaa, S. A. Zvyagin, Y. Sasago, and K. Uchinokura, *Phys. Rev. Lett.* **93**, 087203 (2004).

⁷M. B. Stone, C. Broholm, D. H. Reich, O. Tchernyshyov, P. Vorderwisch, and N. Harrison, *Phys. Rev. Lett.* **96**, 257203 (2006).

⁸M. Kofu, J.-H. Kim, S. Ji, S.-H. Lee, H. Ueda, Y. Qiu, H.-J. Kang, M. A. Green, and Y. Ueda, *Phys. Rev. Lett.* **102**, 037206 (2009).

⁹A. J. Millis and H. Monien, *Phys. Rev. Lett.* **70**, 2810 (1993).

¹⁰A. V. Chubukov and D. K. Morr, *Phys. Rev. B* **52**, 3521 (1995).

¹¹A. W. Sandvik and D. J. Scalapino, *Phys. Rev. Lett.* **72**, 2777 (1994).

¹²T. Dodds, B.-J. Yang, and Y.-B. Kim, *Phys. Rev. B* **81**, 054412 (2010).

¹³M. B. Stone, M. D. Lumsden, S. Chang, E. C. Samulon, C. D. Batista, and I. R. Fisher, *Phys. Rev. Lett.* **100**, 237201 (2008).

¹⁴H. Liao and T. Li, e-print [arXiv:1102.1819](https://arxiv.org/abs/1102.1819).

¹⁵A. Abendschein and S. Capponi, *Phys. Rev. B* **76**, 064413 (2007).

¹⁶A. Collins and C. J. Hamer, *Phys. Rev. B* **78**, 054419 (2008).

¹⁷Y. Matsushita, M. P. Gelfand, and C. Ishii, *J. Phys. Soc. Jpn.* **68**, 247 (1999).

¹⁸D.-k. Yu, Q. Gu, H.-T. Wang, and J.-L. Shen, *Phys. Rev. B* **59**, 111 (1999).

¹⁹T. Roscilde and S. Haas, *Phys. Rev. Lett.* **95**, 207206 (2005).

²⁰K.-K. Ng, F. C. Zhang, and M. Ma, *Phys. Rev. B* **53**, 12196 (1996).

²¹M. P. Gelfand, Z. Weihong, C. J. Hamer, and J. Oitmaa, *Phys. Rev. B* **57**, 392 (1998).

²²K. Gregor and O. I. Motrunich, *Phys. Rev. B* **76**, 174404 (2007).

²³A. W. Sandvik, *Phys. Rev. B* **59**, R14157 (1999); O. F. Syljuåsen and A. W. Sandvik, *Phys. Rev. E* **66**, 046701 (2002).

²⁴B. Kumar, *Phys. Rev. B* **82**, 054404 (2010).

²⁵O. Smirnova, M. Azuma, N. Kumada, Y. Kusano, M. Matsuda, Y. Shimakawa, T. Takei, Y. Yonesaki, and N. Kinomura, *J. Am. Chem. Soc.* **131**, 8313 (2009).

²⁶F. Alet, S. Wessel, and M. Troyer, *Phys. Rev. E* **71**, 036706 (2005).

²⁷E. L. Pollock and D. M. Ceperley, *Phys. Rev. B* **36**, 8343 (1987).

²⁸L. Wang, K. S. D. Beach, and A. W. Sandvik, *Phys. Rev. B* **73**, 014431 (2006).

²⁹M. Campostrini, M. Hasenbusch, A. Pelissetto, P. Rossi, and E. Vicari, *Phys. Rev. B* **65**, 144520 (2002).

³⁰S. Sachdev and R. N. Bhatt, *Phys. Rev. B* **41**, 9323 (1990).

³¹A. V. Chubukov, *Phys. Rev. B* **43**, 3337 (1991).

³²H.-T. Wang, H. Q. Lin, and J.-L. Shen, *Phys. Rev. B* **61**, 4019 (2000).

³³L. Fritz, R. L. Doretto, S. Wessel, S. Wenzel, S. Burdin, and M. Vojta, *Phys. Rev. B* **83**, 174416 (2011).

³⁴S. Gopalan, T. M. Rice, and M. Sgrist, *Phys. Rev. B* **49**, 8901 (1994).

³⁵H. C. Kandpal and J. van den Brink, *Phys. Rev. B* **83**, 140412 (2011).

- ³⁶R. Ganesh, D. N. Sheng, Y.-J. Kim, and A. Paramekanti, *Phys. Rev. B* **83**, 144414 (2011).
- ³⁷H. Mosadeq, F. Shahbazi, and S. A. Jafari, *J. Phys. Condens. Matter* **23**, 226006 (2011).
- ³⁸A. F. Albuquerque, D. Schwandt, B. Hetényi, S. Capponi, M. Mambrini, and A. M. Läuchli, *Phys. Rev. B* **84**, 024406 (2011).
- ³⁹B. K. Clark, D. A. Abanin, and S. L. Sondhi, *Phys. Rev. Lett.* **107**, 087204 (2011).
- ⁴⁰F. Wang, *Phys. Rev. B* **82**, 024419 (2010).
- ⁴¹Y.-M. Lu and Y. Ran, *Phys. Rev. B* **84**, 024420 (2011).
- ⁴²S. Okumura, H. Kawamura, T. Okubo, and Y. Motome, *J. Phys. Soc. Jpn.* **79**, 114705 (2010).
- ⁴³A. Mulder, R. Ganesh, L. Capriotti, and A. Paramekanti, *Phys. Rev. B* **81**, 214419 (2010).
- ⁴⁴E. C. Samulon, Y. Kohama, R. D. McDonald, M. C. Shapiro, K. A. Al-Hassanieh, C. D. Batista, M. Jaime, and I. R. Fisher, *Phys. Rev. Lett.* **103**, 047202 (2009).